Mon. Not. R. Astron. Soc. **000**, ??–?? () Printed 22 June 2016 (MN LATEX style file v2.2)

Constraints on Assembly Bias from Galaxy Clustering

Andrew R. Zentner[1], Andrew Hearin[2], Frank C. van den Bosch[3], Johannes U. Lange[3], and Antonio Villarreal[1]

[1] *Department of Physics and Astronomy & Pittsburgh Particle Physics, Astrophysics, and Cosmology Center (PITT PACC), University of Pittsburgh, Pittsburgh, PA 15260*
[2] *Yale Center for Astronomy & Astrophysics, Yale University, New Haven, CT*
[3] *Department of Astronomy, Yale University, P.O. Box 208101, New Haven, CT*

Today

ABSTRACT

We constrain the newly-introduced decorated Halo Occupation Distribution (HOD) model using SDSS DR7 measurements of projected galaxy clustering, $w_{\rm p}(r_{\rm p})$ of galaxies in r-band luminosity-threshold samples. The decorated HOD is a model for the galaxy–halo connection that augments the traditional HOD by allowing for the possibility of *galaxy assembly bias*: galaxy luminosity may be correlated with dark matter halo properties besides mass, $M_{\rm vir}$. We demonstrate that it is not possible to rule out galaxy assembly bias using DR7 measurements of galaxy clustering alone. Moreover, galaxy samples $M_r < -20, -20.5$ favor strong levels of central galaxy assembly bias. These samples prefer scenarios in which high-concentration halos are more likely to host a central galaxy relative to low-concentration halos of the same $M_{\rm vir}$. We rule out zero assembly bias with high significance for these samples. Satellite galaxy assembly bias is significant for the faintest sample we study, $M_r < -19$. We find no evidence for assembly bias in the $M_r < -21$ sample. Assembly bias should be accounted for in galaxy clustering analyses or attempts to exploit galaxy clustering to constrain cosmology. In addition to presenting the first constraints on HOD models that accommodate assembly bias, our analysis includes numerous improvements over previous analyses of this data set and supersedes previously published results, even in the case of a standard HOD analysis.

1 INTRODUCTION

For more than a decade, halo occupation modeling has been used to interpret large-scale structure measurements and exploit these measurements to constrain galaxy formation models and cosmology (e.g., Yang et al. 2003; Tinker et al. 2005; Zehavi et al. 2005; Porciani & Norberg 2006; van den Bosch et al. 2007; Zheng et al. 2007; Conroy & Wechsler 2009; Yang et al. 2009; Zehavi et al. 2011; Guo et al. 2011; Wake et al. 2011; Yang et al. 2011, 2012; Leauthaud et al. 2012; Rodríguez-Puebla et al. 2012; Tinker et al. 2013; Cacciato et al. 2013; More et al. 2013; Guo et al. 2014; Zu & Mandelbaum 2015). The key assumptions underlying halo occupation modeling are: (1) all galaxies reside in dark matter halos that are biased tracers of the density field; and (2) galaxies occupy halos as a function of halo mass $M_{\rm vir}$ only. In this paper, we present the first analysis of galaxy clustering using a halo occupation model that violates the second of these assumptions and permits galaxies to occupy halos as a function of multiple halo properties.

It is now well known that the strength of halo clustering, the halo bias, depends upon halo properties other than $M_{\rm vir}$ (e.g. Gao et al. 2005; Wechsler et al. 2006; Gao & White 2007; Zentner 2007; Dalal et al. 2008; Lacerna & Padilla 2011), an effect called *halo assembly bias*. If galaxies occupy halos as a function of halo properties other than $M_{\rm vir}$, then standard halo occupation methods will be subject to a systematic error due to *galaxy assembly bias*. Several of us have previously shown that this error can be significant in an analysis of galaxy clustering and can bias inferences about many aspects of galaxy evolution (Zentner et al. 2014).

There is increasing observational evidence that galaxy assembly bias is present in the real Universe. Using an approach based on subhalo abundance matching, Lehmann et al. (2015) showed that the clustering of low-redshift galaxies favors models in which stellar mass depends upon a combination of $M_{\rm vir}$ and halo concentration. Miyatake et al. (2016) and More et al. (2016) have presented evidence for the presence of assembly bias in massive clusters; in particular, they find that clusters with a more centrally concentrated distribution of satellite galaxies cluster more weakly than clusters with more

diffuse satellite galaxy distributions at fixed cluster mass. Indeed, More et al. (2016) suggest that the observed galaxy bias is considerably stronger than had been expected based on N-body simulations coupled with simple models for the galaxy–halo connection, such as subhalo abundance matching. Additional support for the presence of assembly bias has come from a variety of studies that have shown, or suggested, that the large-scale environment of dark matter halos of fixed mass is correlated with the star formation rate of their central galaxies (Yang et al. 2006; Blanton & Berlind 2007; Wang et al. 2008, 2013; Hearin et al. 2014).

Despite this growing evidence, the empirical modeling community has not yet reached a consensus on the question of galaxy assembly bias. For example, Lin et al. (2015) claim that some of the above evidence for assembly bias can be explained by differences in halo mass between the galaxy samples under consideration. Paranjape et al. (2015) urges caution that contamination by satellite galaxies can masquerade as a false signal of assembly bias. Tinker et al. (2008) argue that measurements of void statistics place strong bounds on the possible strength of the signal, though Zentner et al. (2014) constructed an explicit example refuting this claim.

In much of the literature on this topic, the character of the supporting evidence suffers from a severe shortcoming. Until very recently, the only models that have been fit to observational clustering measurements have been traditional models in which assembly bias is assumed from the outset to be zero. Models that include assembly bias such as semi-analytic models are typically too computationally expensive to compare to data in a manner that enables statistical constraints on model parameters (but see Lu et al. 2011, 2012; Henriques et al. 2013; Lu et al. 2014, for recent progress in this direction). Such models are usually compared to data on a case-by-case basis (e.g., Croton et al. 2007), prohibiting any conclusive statement to be made about the strength of any assembly bias signal.

Motivated by this shortcoming, we have developed a new class of empirical models that enable galaxies to occupy halos in a manner that has *simultaneous* dependence upon multiple halo properties (Hearin et al. 2016), *including continuously variable levels of assembly bias*. Crucially, our implementation is of sufficient computational efficiency to permit a proper likelihood analysis of the model parameter space. Armed with this new methodology, in this paper we revisit the interpretation of luminosity-dependent galaxy clustering in the Sloan Digital Sky Survey (SDSS) Data Release 7 (DR7) data, analyzed previously by Zehavi et al. (2011), in the context of both standard halo occupation models and these new models that permit parameterized galaxy assembly bias.

This work presents a re-analysis of the SDSS DR7 data that overcomes numerous shortcomings of previous studies. The primary improvements of our approach stem from the fact that we populate directly halos within a cosmological simulation with mock galaxies, whereas previous analyses relied upon analytical fitting functions with parameters calibrated against a suite of simulations. In direct mock population, delicate issues present in analytic modeling, such as scale-dependent halo bias and halo exclusion, are treated exactly. Our approach also provides a natural framework for studying models of assembly bias, because we can use the exact clustering properties of simulated halos as a function of any arbitrary halo properties in the catalog. It is not necessary to develop new phenomenological models or fitting functions to deal with this additional complexity. With direct mock population, systematic uncertainty in the model is limited to the sample variance of the simulated box, numerical inaccuracies of halo-finding, and errors related to insufficient numerical resolution (e.g., overmerging; Klypin et al. 1999; Behroozi et al. 2013).

In addition to improvements resulting from direct mock population, the simulation we use is based on the latest Planck cosmological parameters (Planck Collaboration et al. 2014), updating previous work. Furthermore, many important differences between this work and the previous analysis by Zehavi et al. (2011) result from the fact that the Monte Carlo Markov Chains used in Zehavi et al. (2011) did not sufficiently sample the posterior distribution (Z. Zheng, private communication). The result is that the constraints in Zehavi et al. (2011) are overly restrictive, considerably so in some cases, and potentially biased. Therefore, *our analysis supersedes previous work even in the case of standard halo occupation models.*

Most importantly, our work demonstrates explicitly that significant assembly bias in M_r-selected samples from SDSS DR7 cannot be ruled out based on a standard analysis of galaxy clustering only. In fact, in agreement with Lehmann et al. (2015), we find that several samples *favor galaxy assembly bias to a degree that is statistically significant.* As demonstrated by Zentner et al. (2014), this conclusion has important consequences for the interpretation of both extant and forthcoming data.

Our paper is organized as follows. In Section 2, we discuss our implementation of halo occupation models and the parameter inference methodology. We present results from both traditional and assembly-biased halo occupation analyses in Section 3. We discuss and interpret our results in Section 4. We summarize our results and draw conclusions in Section 5.

2 METHODS

2.1 Halotools Implementation of HOD Models

To generate predictions for galaxy clustering, we populate dark matter halos with mock galaxies using the publicly-available, open source, `Halotools` software (Hearin et al. 2016). We explore halo occupation distribution (HOD) models in this work (e.g. Seljak 2000; Ma & Fry 2000; Scoccimarro et al. 2001; Berlind & Weinberg 2002), though other techniques that can be used to interpret such data, such as the conditional luminosity function (CLF, e.g., Yang et al. 2003; van den Bosch et al. 2013), exist. In this subsection, we review the "standard" HOD model used in the present work, which assumes that there is no galaxy assembly bias. We refer to such a model as "standard" because all HOD analyses of galaxy clustering to date have assumed no galaxy assembly bias.

In the following subsection, we describe the Decorated HOD model described in Hearin et al. (2016). In both cases, we will only review the salient features of our methodology briefly; interested readers can always refer to `http://halotools.readthedocs.io` and Hearin et al. (2016) for further details.

2.1.1 Simulation

All of our analyses are based on the Bolshoi-Planck (BolshoiP) simulation (Riebe et al. 2011). BolshoiP was run with cosmological parameters based on Planck Collaboration et al. (2014): $\Omega_\Lambda = 0.693; \Omega_\mathrm{m} = 1-\Omega_\Lambda = 0.307; \Omega_\mathrm{b} = 0.048; h = 0.7; \mathrm{n_s} = 0.96$; and $\sigma_8 = 0.82$. BolshoiP simulated the formation of structure within a cubic box 250 Mpc/h on a side, requiring a particle mass of $m_\mathrm{p} = 1.35\times10^8 M_\odot/h$. Further information about the BolshoiP simulation is available at `https://www.cosmosim.org`.

We use publicly available[1] dark matter halo catalogs based on the `ROCKSTAR` halo-finder (Behroozi et al. 2011) and `CONSISTENT TREES` algorithm (Behroozi et al. 2013). In particular, we use the `halotools_alpha_version2` version of the $z = 0$ snapshot of the `'bolplanck'` catalog included with `Halotools`. Halos in these catalogs are defined by the virial radius density contrast given in Bryan & Norman (1998) and have virial masses M_vir within their virial radii. When populating this catalog with mock galaxies, we only use present-day host halos with a value of M_peak that exceeds 300 particles, where M_peak is the maximum mass a halo obtains during its evolution. We consider only host halos and not their subhalos in this work. For host halos, M_peak is almost always nearly identical to the present day virial mass of the halo, M_vir. The minimum peak halo mass considered in our analysis has $M_\mathrm{peak} \geq 4.05\times10^{10}\,h^{-1}\mathrm{M}_\odot$ and this prevents us from analyzing samples with $M_r > -19$. Throughout the remainder of this paper, we will refer only to the virial mass M_vir of the halo to be in closer concordance with other work on HOD analyses.

2.1.2 Occupation statistics

In standard HOD models, central galaxies and satellite galaxies are treated separately, so the model is specified by two probability distributions, one for each type of galaxy. The galaxy-halo connection is specified in terms of $P(N_\mathrm{cen}|M_\mathrm{vir})$ and $P(N_\mathrm{sat}|M_\mathrm{vir})$, the probability that a halo of mass M_vir hosts N_cen central and N_sat satellite galaxies, respectively. $P(N_\mathrm{cen}|M_\mathrm{vir})$ is typically a nearest-integer distribution, as a host halo has only either zero or one central galaxy. Consequently, the occupation statistics of central galaxies are specified by the first moment of $P(N_\mathrm{cen}|M_\mathrm{vir})$, which we model as

$$\langle N_\mathrm{cen}|M_\mathrm{vir}\rangle = \frac{1}{2}\left(1+\mathrm{erf}\left[\frac{\log(M_\mathrm{vir})-\log(M_\mathrm{min})}{\sigma_{\log M}}\right]\right) \quad (1)$$

For every host halo in the catalog we draw a random number from a uniform distribution $\mathcal{U}(0,1)$; for a host halo of present-day virial mass M_vir, a central galaxy is assigned to the halo if the associated random number is less than $\langle N_\mathrm{cen}|M_\mathrm{vir}\rangle$; halos with random values exceeding $\langle N_\mathrm{cen}|M_\mathrm{vir}\rangle$ are left devoid of centrals. The parameter $\log(M_\mathrm{min})$ specifies the halo mass at which the halo has a 50% probability of hosting a central galaxy, while the parameter $\sigma_{\log M}$ specifies the rate at which $\langle N_\mathrm{cen}|M_\mathrm{vir}\rangle$ transitions from zero to unity, with smaller values of $\sigma_{\log M}$ corresponding to a more rapid transition.

We model the distribution $P(N_\mathrm{sat}|M_\mathrm{vir})$ as a Poisson distribution with first moment given by a power law,

$$\langle N_\mathrm{sat}|M_\mathrm{vir}\rangle = \left(\frac{M_\mathrm{vir}-M_0}{M_1}\right)^\alpha. \quad (2)$$

The parameter M_0 allows the power-law to be truncated more rapidly at low masses and we set $\langle N_\mathrm{sat}|M_\mathrm{vir}\rangle = 0$ for $M_\mathrm{vir} < M_0$.

The five parameters of HOD models that are varied in standard analyses are $\log(M_\mathrm{min})$, $\sigma_{\log M}$, α, $\log(M_1)$, and $\log(M_0)$, though, as we show below, central galaxies usually outnumber satellite galaxies by a factor of several, so $\log(M_\mathrm{min})$ and $\sigma_{\log M}$ usually vary along a narrow degeneracy that fixes the total galaxy number density to the observed value. There are many particular choices that can be made for the functional forms of $\langle N_\mathrm{cen}|M_\mathrm{vir}\rangle$ and $\langle N_\mathrm{sat}|M_\mathrm{vir}\rangle$. We have made choices that mimic the standard SDSS DR7 analysis of Zehavi et al. (2011), to expedite comparisons with their results. However, our choice does deviate from Zehavi et al. (2011) in one respect. The mean satellite occupation of Zehavi et al. (2011) is that of Eq. (2) multiplied by an overall factor of $\langle N_\mathrm{cen}|M_\mathrm{vir}\rangle$. We have chosen not to use this as our default because it can introduce difficulties in some analyses (see the discussion of blue galaxy samples in Zentner et al. 2014) and because, as we have verified explicitly, the extra factor introduces only small quantitative changes to our results and no qualitative changes.

2.1.3 Galaxy profiles

Central galaxies in the standard HOD models reside at the halo center, moving with the same velocity as the host halo peculiar velocity. We model the intra-halo spatial distribution of satellite galaxies to be located within R_vir of the halo center, with a spherically symmetric NFW profile (Navarro et al. 1997). The concentration c of each halo's satellite galaxy profile is taken to be the same as the concentration of the dark matter particles in the halo.[2]

We model the radial velocity distribution of satellite galaxies as a Gaussian with first moment equal to the host halo velocity and second moment equal to the solution of the isotropic Jeans equation for an NFW profile (More et al. 2009),

$$\sigma_r^2(\tilde{r}|c) = V_\mathrm{vir}^2\frac{c^2\tilde{r}(1+c\tilde{r})^2}{g(c)}\int_{c\tilde{r}}^\infty \mathrm{d}y\frac{g(y)}{y^3(1+y)^2}, \quad (3)$$

[1] `http://www.slac.stanford.edu/~behroozi/BPlanck_Hlists`

[2] We set a maximum value of $c = 25$ to the NFW concentration, because halos with very large values for the concentration tend to be poorly described by an NFW profile, for example due to a recent merger.

where $\tilde{r} = r/R_{\rm vir}$, $g(x) = \ln(1+{\rm x}) - {\rm x}/(1+{\rm x})$, and $V_{\rm vir}^2 = GM_{\rm vir}/R_{\rm vir}$. We assume that velocities are isotropic, setting the peculiar velocities in each Cartesian direction according to random draws from the above radial velocity distribution.

2.1.4 Predictions for observables

After populating a halo catalog with mock galaxies, we calculate the comoving number density of our mock galaxy sample as $n_{\rm g} = N_{\rm gal}/L_{\rm box}^3$, where $N_{\rm gal}$ is the total number of galaxies in the mock sample. We apply the distant-observer approximation and use the simulation z-axis as the line-of-sight direction, and the distance between points in the xy-plane to define the projected distance $r_{\rm p}$. We place mock galaxies into redshift-space by replacing each galaxy's z-coordinate with $z_{\rm RS} = z + V_{\rm z}/H_0$[3]. Having populated mocks, we perform the computation of the projected two-point galaxy correlation function, $w_{\rm p}(r_{\rm p})$ using the publicly-available `CorrFunc` package (Sinha 2016) which has been extensively optimized for computational speed. We count pairs of points in each of our $r_{\rm p}$ bins, rejecting pairs with line-of-sight distances in redshift space, $\Delta z_{\rm RS}$, exceeding $\pi_{\rm max} = 60$ Mpc/h, which is the same projection depth chosen by Zehavi et al. (2011), both in their analysis of the SDSS DR7 data and in their modeling.

2.2 HOD with Assembly Bias: The Decorated HOD

In addition to the standard occupation statistics described in the previous section, in this paper we also use the decorated HOD formalism to connect galaxies to dark matter halos in a manner that has simultaneous dependence on both $M_{\rm vir}$ and *halo concentration*. Briefly, we use Equations 1 and 2 as our "baseline" first occupation moments. At fixed $M_{\rm vir}$, halos are divided into one of two categories, those of high- and low-concentration, depending on whether the concentration of the halo places it above or below the rank-order percentile $f_{\rm split}$, which we keep fixed to $f_{\rm split} = 0.5$ throughout the paper for simplicity. High-concentration halos have a different first occupation moment relative to low-concentration halos of the same mass,

$$\begin{aligned} \langle N_{\rm gal}|M_{\rm vir}, c_{\rm high}\rangle &= \langle N_{\rm gal}|M_{\rm vir}\rangle + \delta N_{\rm gal} \\ \langle N_{\rm gal}|M_{\rm vir}, c_{\rm low}\rangle &= \langle N_{\rm gal}|M_{\rm vir}\rangle - \delta N_{\rm gal} \end{aligned} \quad (4)$$

This difference, $\delta N_{\rm gal}$, between the first moment of high- and low-concentration halos is modulated by $\mathcal{A}_{\rm bias}$, the novel parameter of the decorated HOD governing assembly bias. Values of $\mathcal{A}_{\rm bias} = \pm 1$ correspond to the maximum strength of assembly bias allowable by the constraint that the model preserves the marginalized first moment, $\langle N_{\rm gal}|M_{\rm vir}\rangle$; thus regardless of the value of $\mathcal{A}_{\rm bias}$, in the decorated HOD the marginalized first moment of centrals and satellites are *unchanged from the baseline value defined by Equations (1) and (2)*. In other words, *decorated HOD models all have the same HODs, when averaged over all halos at fixed mass, as standard HOD models with the same five standard HOD parameters*. The only change in Decorated HOD models is whether or not an additional property also modulates halo occupation at fixed halo mass. A value of $\mathcal{A}_{\rm bias} = 0$ indicates no galaxy assembly bias whatsoever. We refer the reader to Hearin et al. (2016) for further details about the decorated HOD.

In the present work, we fix our model to the simplest class of galaxy assembly bias models, though a recipe for generalizing to more complicated models can be found in Hearin et al. (2016). In particular, we split halos into two populations as specified in the previous paragraph. We then populate halos with satellite galaxies specified by an assembly bias parameter $-1 \leq A_{\rm sat} \leq 1$ and central galaxies with a distinct assembly bias parameter $-1 \leq A_{\rm cen} \leq 1$. For the value of $f_{\rm split} = 0.5$ adopted here, we then have that

$$\begin{aligned} \delta N_{\rm cen} &= A_{\rm cen}\,{\rm MIN}\left[\langle N_{\rm cen}|M_{\rm vir}\rangle, 1 - \langle N_{\rm cen}|M_{\rm vir}\rangle\right] \\ \delta N_{\rm sat} &= A_{\rm sat}\,\langle N_{\rm sat}|M_{\rm vir}\rangle \end{aligned} \quad (5)$$

In our analyses that include assembly bias, we vary these two additional parameters, bringing the total number of parameters that vary in these analyses to seven. As we show below, these additional parameters are in many instances poorly constrained by clustering data of the quality of SDSS DR7 alone, so exploring more complex models of assembly bias does not yet seem justified in such analyses.

2.3 Parameter Inference

We constrain HOD parameters based on SDSS DR7 measurements of the projected galaxy two-point functions, $w_{\rm p}(r_{\rm p})$, and galaxy number densities, $n_{\rm g}$, for luminosity threshold samples published in Zehavi et al. (2011). We use the full covariance matrix of the projected correlation function available at `astroweb.cwru.edu/izehavi/dr7_covar/table8`. We assume a likelihood of the form $\mathcal{L} \propto e^{-\chi^2/2}$, where

$$\chi^2 = \Delta w_{{\rm p},i}\,[C^{-1}]_{ij}\,\Delta w_{{\rm p},j} + \frac{(n_{\rm g}^{\rm mock} - n_{\rm g}^{\rm meas})^2}{\sigma_{\rm n}^2}, \quad (6)$$

$\Delta w_{{\rm p},i} = w_{\rm p}^{\rm mock}(r_{{\rm p},i}) - w_{\rm p}^{\rm meas}(r_{{\rm p},i})$ is the difference between the projected two-point function predicted by the mock catalog and the measured value in the $i^{\rm th}$ separation bin (of 11 bins total), C^{-1} is the inverse of the covariance matrix of the measurements, and repeated indices are summed over. The last term in Eq. (6) is the contribution from the difference between the predicted and measured galaxy number densities. We consider only the eleven values of $w_{\rm p}(r_{\rm p})$ given by Zehavi et al. (2011) in bins logarithmically spaced between $r_{\rm p} = 0.17\,h^{-1}$Mpc and $r_{\rm p} = 16.9\,h^{-1}$Mpc. Though Zehavi et al. (2011) quote values at two larger separations, we find that considering those additional data points adds considerably to the computational expense but alter our results insignificantly. The error on the galaxy number density assumes

[3] A similar exercise is demonstrated as part of the Halotools documentation at `http://halotools.readthedocs.io`

Parameter	Prior Interval
$\log(M_{\rm min})$	[9.0,14.0]
$\sigma_{\log M}$	[0.01,1.5]
$\log(M_0)$	[9.0,14.0]
$\log(M_1)$	[10.7,15.0]
α	[0.0,2.0]
$A_{\rm cen}$	[-1.0,1.0]
$A_{\rm sat}$	[-1.0,1.0]

Table 1. Ranges for the priors used in the parameter inference. All prior distributions are uniform over the specified ranges.

Poisson statistics for both the measured and predicted galaxy number densities.

To infer parameters for the HOD and Decorated HOD models described in the previous subsections, we perform a Markov Chain Monte Carlo (MCMC) sampling of the posterior distribution using the affine-invariant ensemble sampler of Goodman & Weare (2010) as implemented in the `emcee` software package (Foreman-Mackey et al. 2013). For most cases, we find that $\sim 3-10\times10^6$ samples are necessary in order for our chains to converge.

The most important detail of this analysis is the priors on the parameters. In all analyses discussed in this paper, we adopt priors that are uniform distributions over the intervals specified in Table 2.3. In the case of the assembly bias parameters $A_{\rm cen}$ and $A_{\rm sat}$, the priors have strict boundaries. Mathematically, these parameters must satisfy $-1 \leq A_{\rm cen,sat} \leq 1$. Physical considerations require parameter $\sigma_{\log M} > 0$. All other priors have a negligible influence on the posterior aside from $\log M_0$ and $\sigma_{\log M}$. We find that $\log M_0$ is often very poorly constrained by clustering data and priors on $\log M_0$ can have a non-negligible influence on inferred parameters. The parameter $\sigma_{\log M}$ is poorly constrained for the $M_r < -19$ sample.

3 RESULTS

We have performed parameter inference analyses in order to infer the underlying HODs of galaxies from the projected galaxy two-point function $w_{\rm p}(r_{\rm p})$ as described in the preceding section. In this section, we describe the primary results of these analyses. Our marginalized one-dimensional parameter constraints are given in Table 3.1.

3.1 Standard Analysis

Prior to discussing our results using models that include assembly bias, we present results of standard HOD analyses that include no treatment of assembly bias. In our standard HOD analyses, the parameters $\log(M_{\rm min})$, $\sigma_{\log M}$, α, $\log(M_1)$, and $\log(M_0)$ are permitted to vary. The results of the standard HOD analyses and all other analyses are shown in the form of marginalized constraints on individual parameters in Table 3.1. Though the quality of our fits, as measured by the minimum of χ^2 per Degree of Freedom (DoF), varies from case to case, all have a probability $\gtrsim 1\%$ of obtaining a higher value of χ^2 by chance. An example of the inferred posteriors for the HOD parameters is shown in Figure 1 for the sample with $M_r < -20$. We do not show the full posteriors for all five threshold samples in the interest of brevity. The left-hand panels of Figure 2, Figure 3, and Figure 4 show the projected correlation function data along with predictions for $w_{\rm p}(r_{\rm p})$ from 50 randomly-selected models from the MCMC chains within $\Delta\chi^2 \leq 5.89$ of the best-fit model. Under the assumption of a Gaussian posterior distribution, $\Delta\chi^2 = 5.89$ contains 68% of the posterior probability for a five-parameter model. Note that the significant covariance in the data makes it difficult to determine the quality of fits from visual inspection of these figures.

Our parameter constraints can be compared to the standard HOD analysis performed by Zehavi et al. (2011) by examining the top two rows in each luminosity threshold grouping in Table 3.1. In all cases, we quote the medians of our posteriors as our central values and our, generally asymmetric, errorbars, give the $16^{\rm th}$ and $84^{\rm th}$ percentiles of the posterior samples so as to correspond roughly with "$1-\sigma$" errors. The inferred parameters from our standard analyses differ in several ways from the Zehavi et al. (2011) analysis. Firstly, in our re-analysis of the projected clustering data, we generally find all mass scales to be slightly higher than in the work of Zehavi et al. (2011). This difference is primarily due to the slightly different cosmological model used in this work as compared to that of Zehavi et al. (2011). The most important differences are in the values of $\Omega_{\rm M}$, and σ_8. Zehavi et al. (2011) assumed $\Omega_{\rm M} = 0.25$ and $\sigma_8 = 0.8$, whereas in the present work, we use the BolshoiP simulation in which $\Omega_{\rm M} = 0.307$ and $\sigma_8 = 0.82$. Slightly larger mass scales are necessary in an analysis with higher $\Omega_{\rm M}$ and σ_8 in order to maintain galaxy number densities fixed with larger halo number densities. A detailed comparison between our central values and those of Zehavi et al. (2011) is further confounded by the fact that we use a virial halo definition, whereas the analytic model of Zehavi et al. (2011) has been calibrated to friend-of-friends halo masses (Z. Zheng, Private Communication).

A second noteworthy difference between the present work and that of Zehavi et al. (2011) is that we find many parameters to be notably more poorly constrained. At the lower luminosity thresholds, for example, we constrain $\log(M_{\rm min})$ and $\sigma_{\log M}$ with several times lower precision than Zehavi et al. (2011). We do not show our constraints on $\log(M_0)$ as they are very poor, with 1-sigma constraints $\gtrsim 1$ dex for all samples. In several cases, the constraint on $\log(M_0)$ is determined by the prior given in Table 2.3. This is in stark contrast to several of the results of Zehavi et al. (2011). For example, for the threshold sample with $M_r < -19.5$ ($M_r < -20.5$), Zehavi et al. (2011) quote $\log(M_0) = 12.23 \pm 0.17$ (12.35 ± 0.24), whereas we infer $\log(M_0) = 11.38^{+0.95}_{-1.57}$ ($11.19^{+0.89}_{-1.39}$). Examining the form of Eq. (2), it is sensible that the parameter $\log(M_0)$ should be unconstrained at the lower end, because the value of M_0 does not alter the predicted satellite number once $M_0 \ll M_1$. The tighter constaints are

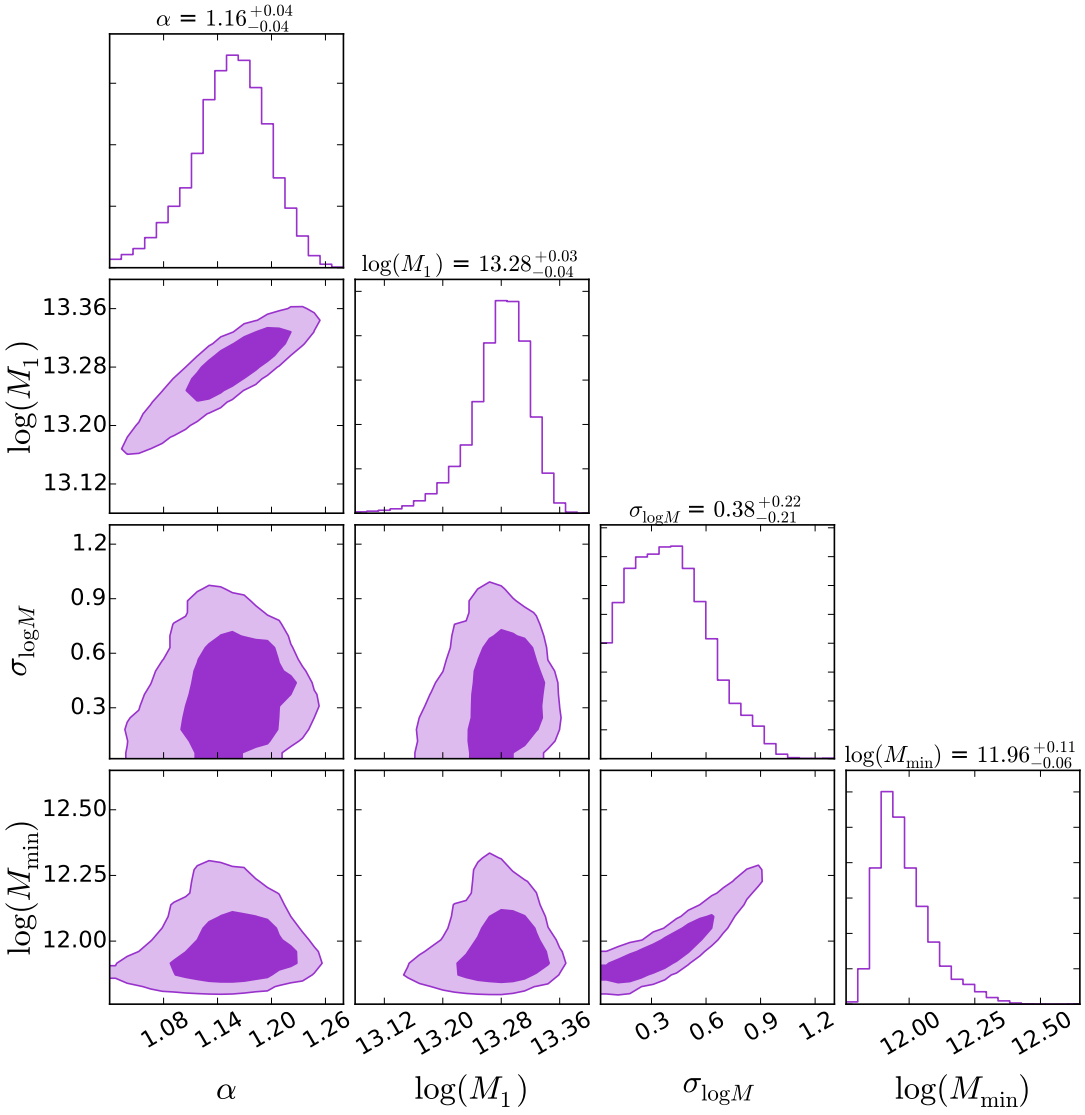

Figure 1. Two-dimensional marginalized constraints on HOD parameters inferred from standard HOD fits to $w_{\rm p}(r_{\rm p})$ data for the $M_r < -20$ sample. The HOD parameter $\log(M_0)$ is extremely poorly constrained by the $w_{\rm p}(r_{\rm p})$ data and has been omitted. The inner contours contain 68% of the posterior probability while the outer contours contain 95% of the probability. The panels along the diagonal show the one-dimensional, marginalized posteriors on each of these parameters. The values above each panel on the diagonal show the median value for the parameter in our chains along with the $16^{\rm th}$ and $84^{\rm th}$ percentiles.

also particularly puzzling given that Zehavi et al. (2011) adopt an arbitrary 5% error on all galaxy number density measurements, an error that greatly exceeds the Poisson error, typically $< 1\%$, that we adopt. This additional error contribution also limits the value of comparing our χ^2 values with those of Zehavi et al. (2011), as the latter values will be artificially lower.

We have confirmed with one of the authors of Zehavi et al. (2011) that the MCMC chains used in a number of their analyses may not have been properly converged and that this may have led to a significant underestimation of the uncertainties on the inferred parameters, especially $\log(M_0)$, $\log(M_{\rm min})$, and $\sigma_{\log M}$. The analysis of Zehavi et al. (2011) used 10^4 samples, whereas we find that several $\times 10^5$ to 10^6 samples are often necessary for convergence. In all cases, our final results are from $> 10^6$ samples of the posterior. The cause of the problem is likely a restrictive proposal distribution that causes the chain to diffuse through the posterior distribution only extremely slowly (Z. Zheng, Private Communication). We have recreated qualitatively similar behavior considering only small subsets of our full MCMC chains. Consequently, insufficient sampling of the posterior seems to be the likely resolution of the discrepancies between our work and that of Zehavi et al. (2011).

Two degeneracies are manifest in Fig. 1 that are common to all of our analyses. The parameters $\log(M_1)$ and α are degenerate with each other and positively correlated. The parameter M_1 is the mass scale at which a halo has one satellite on average, and α is the power-law

Sample M_r	Authors	$\log(M_{\rm min})$	$\sigma_{\log M}$	$\log(M_1)$	α	$A_{\rm cen}$	$A_{\rm sat}$	χ^2/DoF
-21	Zehavi+11	12.78 ± 0.10	0.68 ± 0.15	13.80 ± 0.03	1.15 ± 0.06	$--$	$--$	3.1
-21	Zentner+16	$12.93^{+0.07}_{-0.10}$	$0.74^{+0.09}_{-0.13}$	$13.96^{+0.03}_{-0.05}$	$1.27^{+0.08}_{-0.10}$	$--$	$--$	1.59
-21	Zentner+16	$12.83^{+0.11}_{-0.09}$	$0.60^{+0.15}_{-0.17}$	$13.93^{+0.05}_{-0.08}$	$1.16^{+0.12}_{-0.14}$	$0.29^{+0.44}_{-0.35}$	$0.08^{+0.49}_{-0.36}$	1.34
-20.5	Zehavi+11	12.14 ± 0.03	0.17 ± 0.15	13.44 ± 0.03	1.15 ± 0.03	$--$	$--$	2.7
-20.5	Zentner+16	$12.25^{+0.07}_{-0.03}$	$0.23^{+0.17}_{-0.15}$	$13.59^{+0.02}_{-0.02}$	$1.20^{+0.04}_{-0.04}$	$--$	$--$	1.90
-20.5	Zentner+16	$12.32^{+0.13}_{-0.08}$	$0.45^{+0.21}_{-0.25}$	$13.59^{+0.04}_{-0.04}$	$1.14^{+0.05}_{-0.06}$	$> 0.08(90\%)$ $> 0\,(92.3\%)$	$0.22^{+0.40}_{-0.31}$	1.40
-20	Zehavi+11	11.83 ± 0.03	0.25 ± 0.11	13.08 ± 0.03	1.00 ± 0.05	$--$	$--$	2.1
-20	Zentner+16	$11.96^{+0.11}_{-0.06}$	$0.38^{+0.22}_{-0.21}$	$13.28^{+0.03}_{-0.04}$	$1.16^{+0.04}_{-0.04}$	$--$	$--$	1.88
-20	Zentner+16	$12.24^{+0.29}_{-0.21}$	$0.84^{+0.37}_{-0.31}$	$13.19^{+0.06}_{-0.08}$	$1.05^{+0.06}_{-0.08}$	$> 0.29(99\%)$ $> 0\,(99.9\%)$	$0.01^{+0.35}_{-0.27}$	1.09
-19.5	Zehavi+11	11.57 ± 0.04	0.17 ± 0.13	12.87 ± 0.03	0.99 ± 0.04	$--$	$--$	1.00
-19.5	Zentner+16	$11.76^{+0.33}_{-0.11}$	$0.51^{+0.51}_{-0.29}$	$13.05^{+0.04}_{-0.08}$	$1.12^{+0.04}_{-0.07}$	$--$	$--$	1.24
-19.5	Zentner+16	$11.80^{+0.36}_{-0.16}$	$0.63^{+0.53}_{-0.37}$	$13.04^{+0.09}_{-0.12}$	$1.06^{+0.07}_{-0.10}$	$> -0.01(84\%)$	$> -0.16(84\%)$	0.69
-19	Zehavi+11	11.45 ± 0.04	0.19 ± 0.13	12.64 ± 0.04	1.02 ± 0.02	$--$	$--$	1.8
-19	Zentner+16	$11.72^{+0.33}_{-0.19}$	$0.70^{+0.51}_{-0.45}$	$12.78^{+0.04}_{-0.04}$	$1.03^{+0.04}_{-0.04}$	$--$	$--$	2.67
-19	Zentner+16	$11.62^{+0.33}_{-0.13}$	$0.53^{+0.57}_{-0.35}$	$12.83^{+0.06}_{-0.07}$	$1.02^{+0.04}_{-0.04}$	$0.35^{+0.45}_{-0.66}$	$> 0.02(84\%)$ $> 0\,(85\%)$	2.01

Table 2. Results of standard HOD fits to SDSS DR7 $w_{\rm p}(r_{\rm p})$ as well as fits using a parameterized model of assembly bias. Assembly bias is quantified by the parameters $A_{\rm cen}$ ($A_{\rm sat}$) for central (satellite) galaxies. The secondary property that we assume to determine the galaxy HOD is halo concentration. $A_{\rm cen,sat} = 0$ means that there is no assembly bias while $A_{\rm cen,sat} = 1$ ($A_{\rm cen,sat} = -1$) means that galaxy abundance is maximally correlated (anticorrelated) with halo concentration at fixed $M_{\rm vir}$. Thus the $A_{\rm cen,sat}$ parameters span the range $[-1, 1]$. If the constraints on $A_{\rm cen}$ and $A_{\rm sat}$ are unspecified in the table, then the model used to interpret the data does not include assembly bias. In our analyses, quoted parameter values with errors correspond to the median value of the parameter and the $16^{\rm th}$ and $84^{\rm th}$ percentiles. In cases for which the posterior on $A_{\rm cen,sat}$ is significant at the boundary of the permissible parameter range (e.g., $A_{\rm cen}$ for $M_r < -20$), we provide one-sided constraints. In the cases exhibiting the strongest assembly bias, we also quote the probability with which the inferred value of $A_{\rm cen,sat}$ exceeds zero.

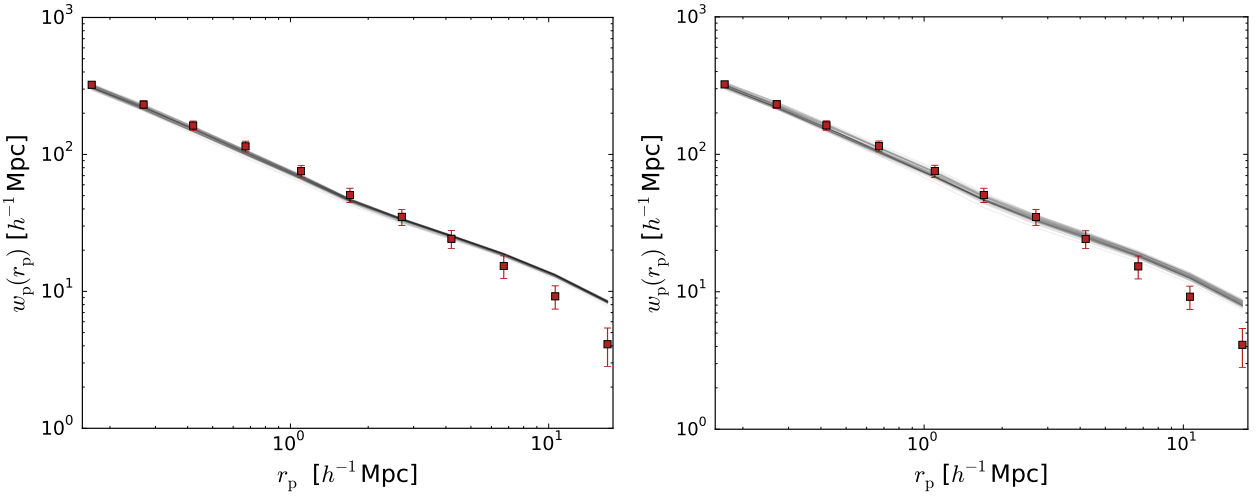

Figure 2. Left: The $M_r < -19$ threshold sample projected correlation function with diagonal elements of covariance (points with errorbars). The grey lines are 50 randomly-selected HOD models that yield $\Delta\chi^2 < 5.89$ compared to the best-fitting model. For a Gaussian posterior distribution, $\Delta\chi^2 = 5.89$ would contain 68% of the probability in the full five-dimensional parameter space. **Right:** Same as the left panel but using a fit to a Decorated HOD model that contain parameters to describe the strength of assembly bias.

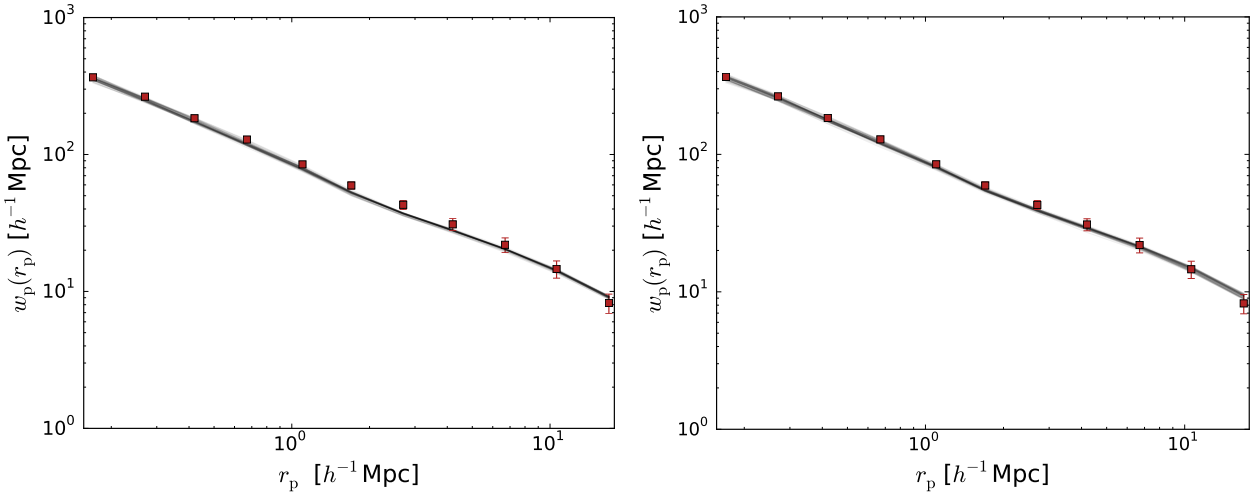

Figure 3. The same as Figure 2, but for the $M_r < -20$ threshold sample.

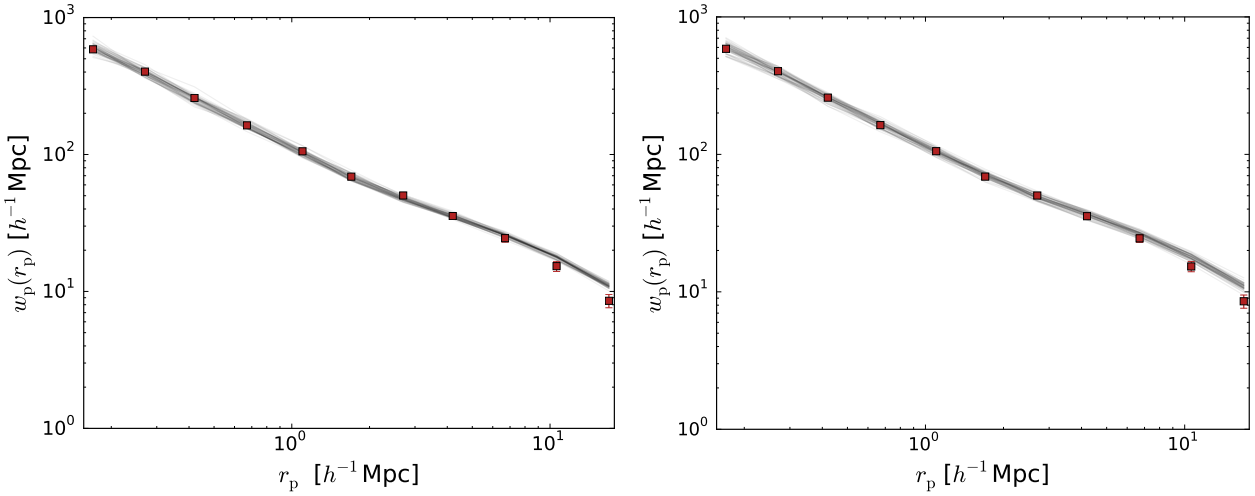

Figure 4. The same as Figure 2, but for the $M_r < -21$ threshold sample.

index describing the dependence of average satellite number on halo mass. Increasing M_1 *decreases* the number of satellites in massive halos by increasing the mass scale where the power law abundance becomes operative. An increase in α can partly compensate for an increase in M_1 by increasing the rate at which average satellite number grows with halo mass.

Look for the purple banana[4] in the third panel from the left in the bottom row of Figure 1. This panel illustrates that the parameters $\log(M_{\rm min})$ and $\sigma_{\log M}$ share a relatively narrow degeneracy as well. This degeneracy is largely induced by the measured number density of the sample. Increasing $\log(M_{\rm min})$ decreases galaxy number density, but this can be compensated by an increase in $\sigma_{\log M}$, which places galaxies in a fraction of the considerably more numerous halos with masses less than $M_{\rm min}$. The consequence is that $\log(M_{\rm min})$ and $\sigma_{\log M}$ are degenerate with each other such that most of the posterior probability lies in a narrow band along which $\log(M_{\rm min})$ and $\sigma_{\log M}$ are positively correlated. In the following plots, we exclude the parameter $\sigma_{\log M}$, in order to increase the clarity of the plots, because the viable range of $\sigma_{\log M}$ is determined by this simple degeneracy with $\log(M_{\rm min})$. Our constraints on $\sigma_{\log M}$ are listed in Table 3.1.

The results of this subsection demonstrate that we achieve reasonable fits to projected galaxy clustering data using direct HOD population of a high-resolution numerical simulation of structure formation. These results also update and supersede existing constraints in the literature in at least three respects. First, we work within the best-fit Planck cosmology. Second, we perform our parameter inference analysis using direct population of halos identified in a numerical simulation of cosmological structure formation (BolshoiP). This greatly mitigates

[4] 'Til they put us in the truck.

modeling uncertainties associated with nonlinear density field evolution, scale-dependent halo bias, halo exclusion, or other effects that have been difficult to incorporate into analytical halo models with high precision (e.g., van den Bosch et al. 2013, and references the). Third, we have explored the posteriors of the parameters with significantly more samples (roughly two orders of magnitude), thereby mitigating errors on inferred parameters caused by insufficient sampling of the posterior by Zehavi et al. (2011).

3.2 Analysis with Decorated HOD

We turn now to a discussion of our parameter inference analysis of projected galaxy clustering in decorated HOD models that include a treatment of galaxy assembly bias. In this work, we consider only the simplest model of galaxy assembly bias, introducing only two new parameters, $A_{\rm cen}$ and $A_{\rm sat}$, that describe the strength of central galaxy and satellite galaxy assembly bias respectively. These parameters are limited to values of $-1 \leq A_{\rm cen,sat} \leq 1$, and $A_{\rm cen,sat} = 0$ when there is no galaxy assembly bias. In this work, we use halo concentration as our secondary halo property, so $A_{\rm cen,sat} = 1$ ($A_{\rm cen,sat} = -1$) means that the mean number of galaxies per halo is maximally correlated (anti-correlated) with halo concentration. The model and its implementation in `Halotools` is discussed further in Section 2.2 above and in more detail in Hearin et al. (2016).

Examples of our fits are given in the right-hand panels of Figure 2, Figure 3, and Figure 4. The general trend that can be gleaned from these figures is that introducing assembly bias improves the fit to the measured two-point functions across the transition from the one-halo (highly nonlinear) to two-halo (nearly linear) regimes near $r_{\rm p} \sim 2\,h^{-1}$Mpc, an effect that could be anticipated by the known scale-dependence of galaxy assembly bias (Sunayama et al. 2016). This is most apparent for the $M_r < -20$ threshold sample shown in Fig. 3. Visually, these differences appear to be small; however, Table 3.1 shows that they are statistically important.

The one-dimensional marginalized constraints on all parameters from these analyses are given in the lowest row of each luminosity threshold grouping in Table 3.1. In cases where the posterior distribution of either $A_{\rm cen}$ or $A_{\rm sat}$ contains significant probability at the limits of the parameter range (e.g., see the posterior distribution for $A_{\rm cen}$ in Fig. 6), we quote one-sided constraints. Examples of one- and two-dimensional visualizations of the posteriors from our analyses are shown in Figure 5, Figure 6, and Figure 7 for the $M_r < -19$, $M_r < -20$, and $M_r < -21$ samples respectively.

Table 3.1 and Figures 5–7 all make several simple, generic points. Introducing additional parameter freedom associated with galaxy assembly bias generally increases the volume of the viable parameter space, even for the subset of five standard HOD parameters. Constraints on the standard HOD parameters are generally less restrictive in models that include assembly bias. This is exactly what is expected from the introduction of additional parameter freedom.

Focusing attention on the parameters describing galaxy assembly bias, it is evident that these parameters are often quite poorly constrained by galaxy clustering data. This is important as it implies that galaxy clustering of the precision of SDSS DR7 measurements cannot rule out, or strongly restrict, galaxy assembly bias in many cases. This is the case, for example, for the $M_r < -21$ sample with posteriors shown in Fig. 7. In this case, both $A_{\rm cen}$ and $A_{\rm sat}$ have posteriors that peak near zero, but are very broad. Nonetheless, it is apparent that the presence of galaxy assembly bias can alter the inferred HOD, or more generally, the inferred relationship between galaxies and halo mass. This is most evident for the $M_r < -20$ threshold sample, for which there are significant differences in the inferred values of all baseline HOD parameters between models with and without galaxy assembly bias. Other threshold samples exhibit significant differences particularly for α, and to a lesser degree for $\log(M_{\rm min})$ and $\sigma_{\log M}$.

Beyond those generic conclusions, a few specific cases are worthy of further examination. Consider the $M_r < -20$ sample. The inferred value of $A_{\rm cen} > 0.28$ at 99% confidence. In this case the data strongly prefer $A_{\rm cen} > 0$ ($A_{\rm cen} > 0$ at 99.9%) and thus strongly prefer galaxies to reside in halos of larger concentration at fixed halo mass. Figure 8 compares the inferred HODs for the $M_r < -20$ sample in a standard HOD analysis with the inferred HOD from our decorated HOD analysis that includes parameters to describe assembly bias. The bands in purple rein in the region of HODs for models within $\Delta\chi^2 \leq 5.89$ of the best-fit model. This is an explicit example of the degree to which the inferred relationship between galaxies and halos can be altered by assembly bias. In the assembly-biased case, the efficiency of forming a sufficiently luminous galaxy is a function that increases slowly over nearly two decades in halo mass in contrast to a standard analysis HOD where this efficiency rises rapidly over roughly one third of a decade in $M_{\rm vir}$. Taking these results at face value, the reason that the HOD of central galaxies can vary slowly over several orders of magnitude in $M_{\rm vir}$ is that larger galaxies form more efficiently in high-concentration halos at fixed mass.

Though the evidence for assembly bias is the most significant for the $M_r < -20$ sample, there are hints of galaxy assembly bias in other samples. Satellite galaxies show a marginal preference for occupying halos of higher concentration in the $M_r < -19$ threshold sample, with $A_{\rm sat} > 0$ at 85%. The $M_r < -19.5$ sample exhibits weak preference for a positive correlation of galaxy occupation with halo concentration at fixed mass for both satellite galaxies and central galaxies. The low value of χ^2 in this case is also suggestive of possible over-fitting using these additional parameters (but see the discussion in the subsequent paragraph). Continuing upward with luminosity, the $M_r < -20.5$ sample exhibits a significant preference for central galaxy assembly bias, with $A_{\rm cen} > 0$ at 92.3%. Lastly, there is no preference for either central galaxy or satellite galaxy assembly bias for the $M_r < -21$ threshold sample, for which both $A_{\rm cen}$ and $A_{\rm sat}$ are consistent with zero well within 1σ. While we give a brief discussion of these results in the following section, the implications of all of these results, particularly for quantities derived from HODs, are far too numerous to address compre-

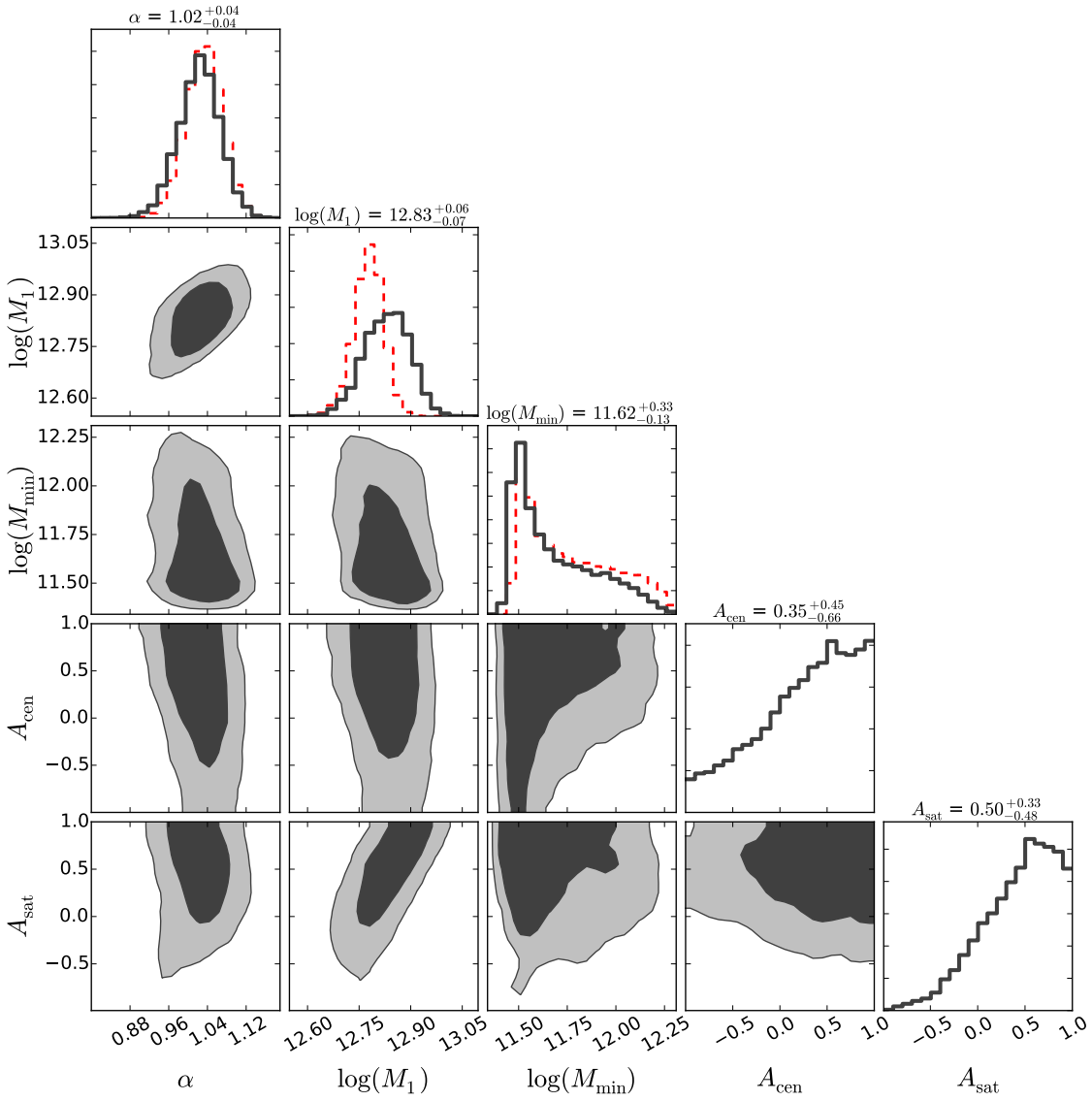

Figure 5. Two-dimensional marginalized constraints on decorated HOD parameters inferred from fits to $w_{\rm p}(r_{\rm p})$ data for the $M_r < -19$ sample. The contours and histograms along the diagonal panels are as in Fig. 1. The dashed line in the panels along the diagonal show the posteriors on these parameters from the standard analysis without any parameterization of galaxy assembly bias. In these panels, both histograms are normalized to the same total probability. The decorated HOD models include a two-parameter model for assembly bias. The HOD parameter $\log(M_0)$ is extremely poorly constrained by the data and we omit it for clarity. Likewise, as in Fig. 1, $\sigma_{\log M}$ and $\log(M_{\rm min})$ share a narrow degeneracy, so we have suppressed $\sigma_{\log M}$ in order to make constraints on other parameters more easily visible.

hensively in the present manuscript; however, we plan to address them in forthcoming publications.

In addition to fitting model parameters, it is possible to ask whether or not the fits to the data warrant the use of additional parameters (in this case, the two parameters used to describe assembly bias). This requires a metric that penalizes the use of additional parameters. A commonly-used metric is the Bayesian Information Criterion (BIC, Schwarz 1978), defined as

$$\mathrm{BIC} = -2\mathcal{L}_{\rm max} + k \ln N, \qquad (7)$$

where $\mathcal{L}_{\rm max}$ is the maximum of the likelihood, k is the number of parameters in the model and N is the number of data points. We compute the change in the BIC, ΔBIC, by subtracting the BIC for the analysis with assembly bias from the BIC in the standard analysis in which there is no assembly bias. With this convention, $\Delta\mathrm{BIC} > 0$ favors assembly bias, suggesting that the data warrant the additional parametric freedom. Conversely, $\Delta\mathrm{BIC} < 0$ favors the standard analysis, suggesting that the additional freedom in the model does not improve the description of the data to a sufficiently great degree to support the added complexity. A common convention is to refer to the preference as *strong* when $|\Delta\mathrm{BIC}| \geq 5$.

The values of ΔBIC are given in Table 3.2. In the analysis of the $M_r < -21$ sample, $\Delta\mathrm{BIC} < 0$, indicat-

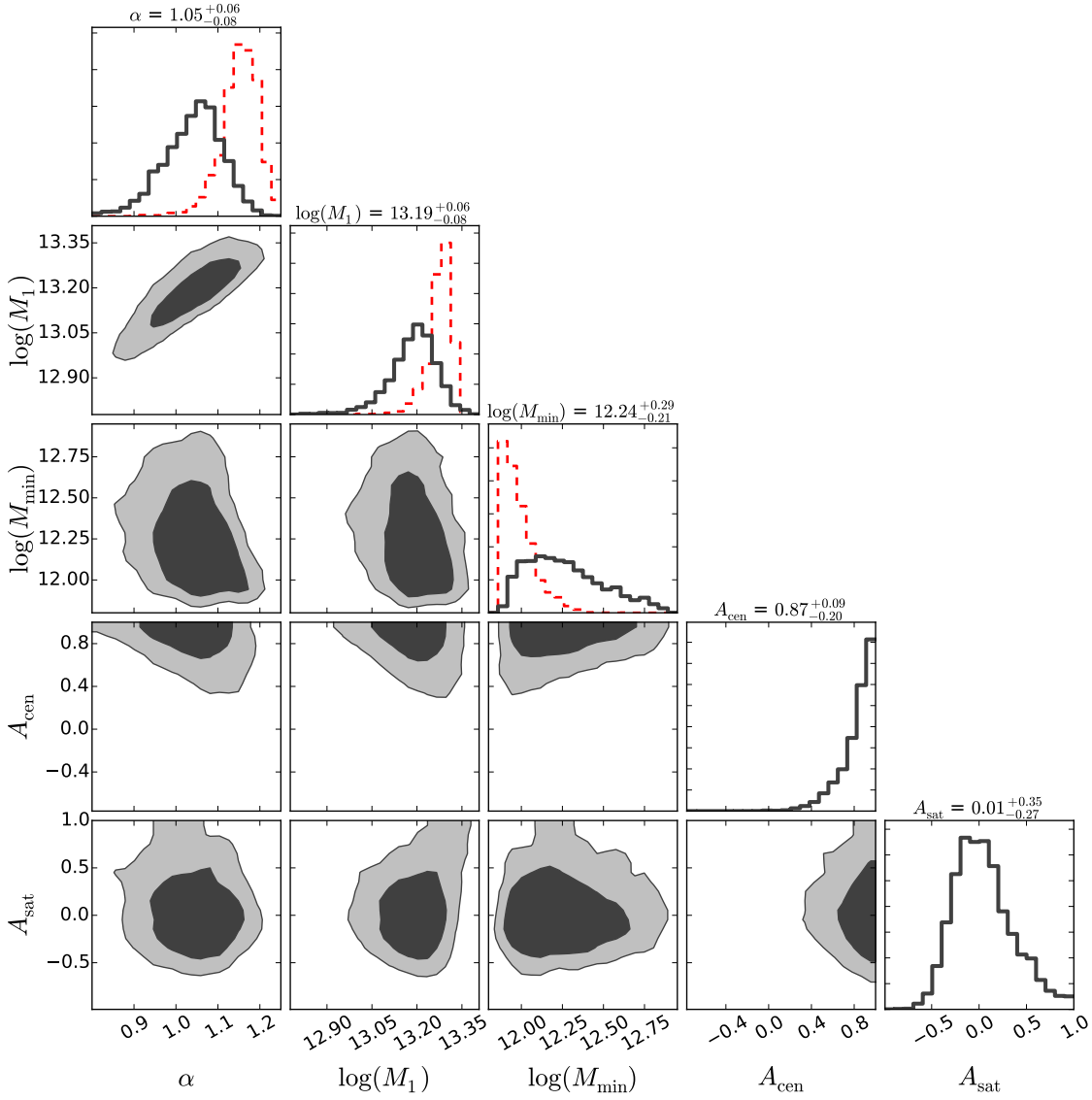

Figure 6. The same as Figure 5, but for the $M_r < -20$ sample.

M_r Threshold	ΔBIC
-21	-0.54
-20.5	1.33
-20	2.88
-19.5	0.26
-19	3.78

Table 3. Change to the Bayesian Information Criterion, ΔBIC, after introducing additional parametric freedom to accommodate galaxy assembly bias. Sign convention is such that positive values favor models including assembly bias, negative values favor standard HOD models with no assembly bias parameters. Changes in the Bayesian Information Criterion $|\Delta\text{BIC}| \geq 5$ strongly favor one model over another. None of the models we explore achieve this threshold.

ing that the additional parameters describing assembly bias are not warranted by the data. For all other samples, $\Delta\text{BIC} > 0$, showing a preference for the models with assembly bias. The cases that most support the additional complexity of the decorated HOD are $M_r < -19$ and $M_r < -20$, for which ΔBIC is considerable, but in no case does the ΔBIC rise to the conventional level for *strong* preference.

4 INTERPRETATION

The results of the previous section suggest that halo mass is insufficient to predict the galaxy content of a halo to the precision mandated by an analysis of SDSS DR7 clustering measurements (particularly the $M_r < -19$, $M_r < -20$, and $M_r < -20.5$ samples). This should not be surprising, as the process of galaxy formation and evolution is complex and there is little reason to suspect that

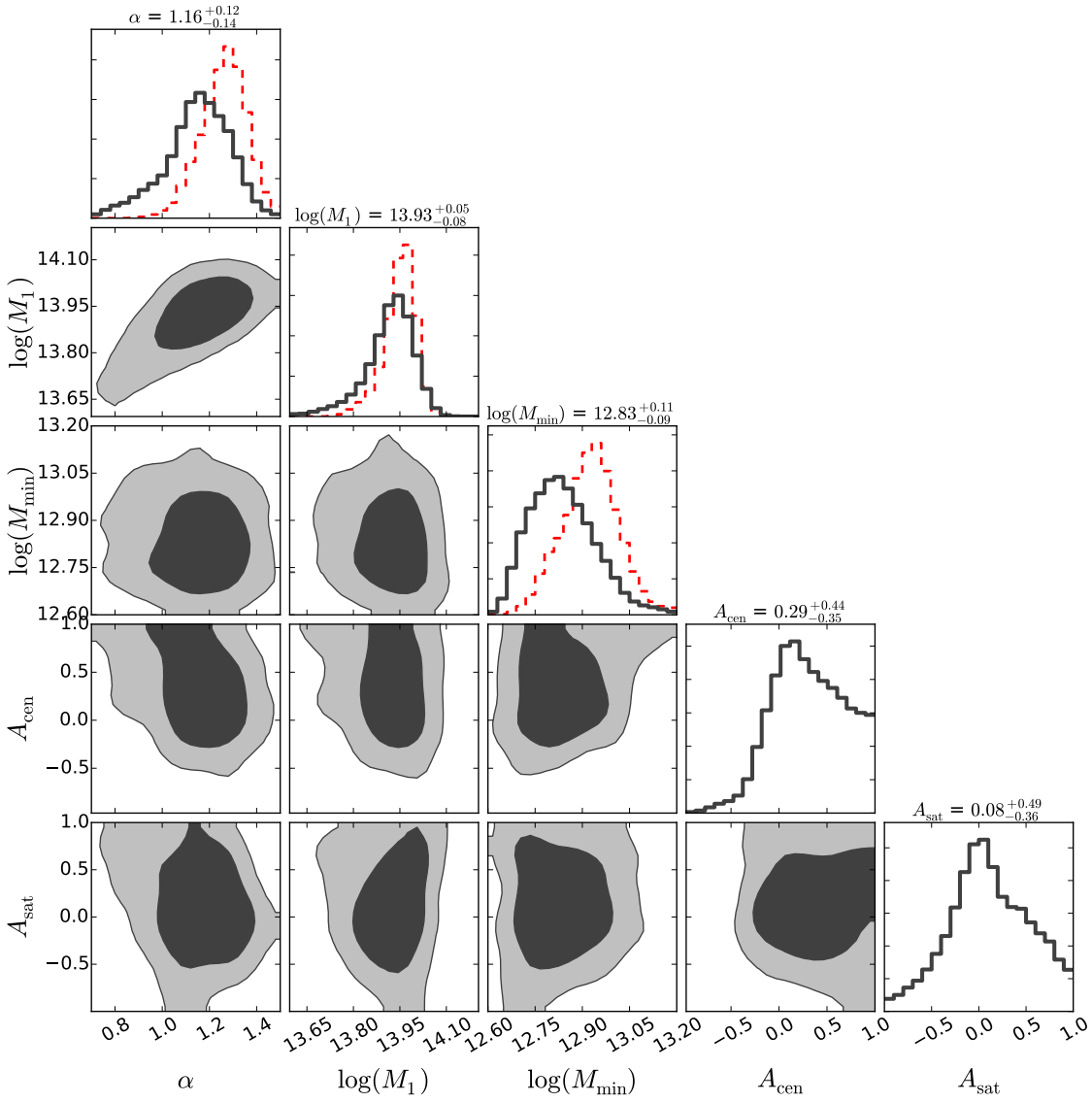

Figure 7. The same as Figure 5, but for the $M_r < -21$ sample.

all potentially-important factors are determined by a single halo property. Our results further suggest that halo concentration (or some other halo property correlated with halo concentration) impacts the galaxy content of a halo, at least for galaxies of some luminosities. In particular, the assembly bias inferred from the $M_r < -20$ and $M_r < -20.5$ samples suggests that galaxies in roughly Milky Way-sized halos tend to be more luminous if they reside in halos with higher-than-average concentrations.

Within the context of the standard model of structure formation, this can be interpreted in at least two ways that are not mutually exclusive. Although our analysis cannot support either of these scenarios unambiguously, they are reasonable starting points for further consideration. One possibility is simply that the growth and structure of the host halo itself may drive this luminosity-concentration dependence. For example, halos of higher concentration at fixed mass have deeper potential wells (specifically, higher escape velocities from the halo center). Therefore, gravity more strongly binds the stellar and gaseous contents of such halos possibly driving more rapid star formation or making the galaxies less susceptible to feedback mechanisms that suppress star formation. Higher concentration halos have also formed earlier, on average (e.g., Wechsler et al. 2002). This suggests that any physics that acts upon the baryonic content of the halo and its high-density environment may have been operative for a longer time, resulting in a larger, more luminous galaxy. Concentration-dependent halo assembly bias persists to very large separations ($r > 10\,h^{-1}$Mpc, e.g., Wechsler et al. 2006) and this picture can therefore accommodate galaxy assembly bias on such large scales.

Another possible explanation for having more luminous galaxies reside in higher concentration halos is halo-halo interactions. Recent work on halo evolution suggests that a more physical definition of the size of a halo should

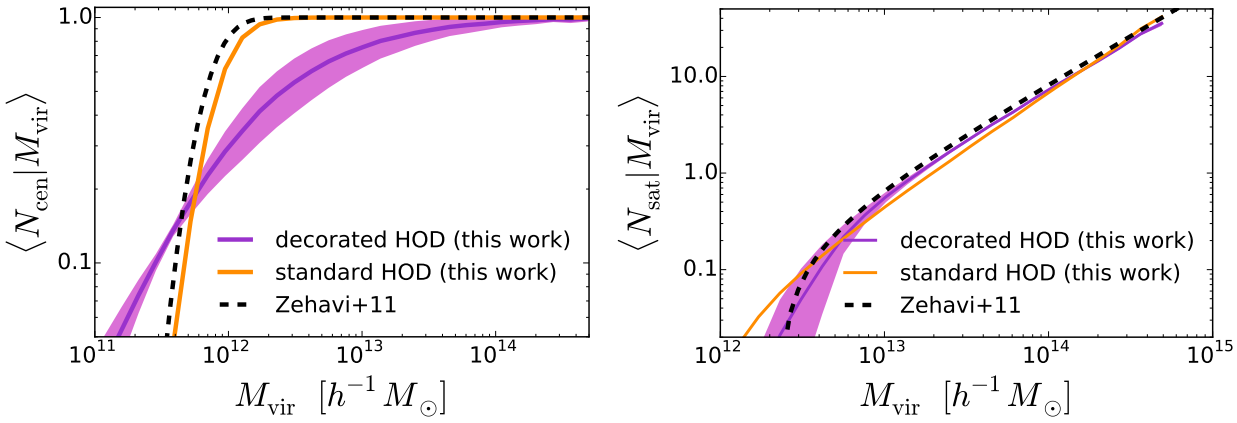

Figure 8. The first moments of the central (left panel) and satellite (right) occupation distributions from the best-fit models to the $M_r \leq -20$ sample. The solid, purple curve shows the HOD of our best-fit model that includes the effect of assembly bias; the solid, orange curve shows the HOD of the best-fit model in which assembly bias is assumed to be zero; the dashed, black curve shows the best-fit HODs from Zehavi et al. (2011). The light purple error band around the decorated HOD results contains 68% of all samples of the posterior within $\Delta\chi^2 \leq 5.89$ of the best-fit model at each bin of halo mass. For any individual model, the values of the HOD at each mass point are obviously correlated and do not vary independently from one mass bin to another.

be $\sim 2-3$ times the traditional virial radius (Wetzel et al. 2014; Adhikari et al. 2014; Wetzel & Nagai 2015; More et al. 2015; Sunayama et al. 2016). This "splashback radius" incorporates "splashback" halos that have passed within the dense environment of the central halo, but are traditionally classified as distinct halos despite being strongly influenced by the environment of the central halo. Wang et al. (2009), Wetzel et al. (2014), and Sunayama et al. (2016), all find that these "splashback" halos are a significant cause of halo assembly bias on scales $r \sim 1-3\,h^{-1}$Mpc, where assembly bias is most pronounced and strongly scale dependent. Consequently, decorated HOD models exhibit this same feature (Hearin et al. 2016), and is not a coincidence that the greatest improvement of the decorated HOD in the description of galaxy clustering occurs on these same length scales (see Fig. 2-4 and the associated discussion).

This "splashback" hypothesis has further merit in that it has the same sense as suggested by the data. Splashback halos have experienced mass loss as a consequence of their tidal interactions with a larger, nearby halo. As a consequence, splashback halos are expected to be less massive than 'regular' host halos that host similar galaxies (Dalal et al. 2008). Meanwhile, high concentrations are a hallmark of splashback halos (Sunayama et al. 2016). The implication is a population of halos, correlated on scales $r \sim 1-3\,h^{-1}$Mpc, that have concentrations that are high for their mass and galaxies that are overluminous for their mass. This is precisely the sense of assembly bias suggested by our analysis. Note, though, that this splashback effect cannot explain galaxy assembly bias on large, linear scales.

Our formulation of the Decorated HOD is not designed to address the finer-grained causes for observed correlations. Rather, what we have provided in this work is a robust boundary condition that more detailed specific models, such as semi-analytical models and hydrodynamical simulations, should satisfy. However, we reiterate an important corollary to our findings. Although SDSS projected clustering measurements favor strong levels of assembly bias, the constraints on even our simple $\mathcal{A}_{\rm bias}$ parameters are relatively weak. This implies that *it may not be possible to constrain a finer-grained physical picture using projected clustering at a level that is interesting.* In order to constrain models that are more complex than simple empirical models such as the Decorated HOD, it is necessary to leverage additional constraining power of observations beyond two-point clustering.

5 CONCLUSIONS

We have re-analyzed the SDSS DR7 measurements of projected galaxy clustering, $w_{\rm p}$, and number density, $n_{\rm g}$, originally published in Zehavi et al. (2011). The novelty of our work is that we have performed these analyses using the decorated Halo Occupation Distribution (HOD) formalism, which allows for galaxy assembly bias and was introduced by Hearin et al. (2016) precisely for this purpose. In this work, we provide the first quantitative constraints on assembly bias derived from the Decorated HOD. Projected galaxy clustering, $w_{\rm p}(r_{\rm p})$ is already very well-measured within SDSS DR7, therefore it is likely that further improvements on assembly bias constraints at low-redshift will require the use of additional observables such as galaxy–galaxy lensing, group statistics, void statistics, or numerous other possibilities. We are currently exploring many of those possibilities and will report on those results in forthcoming publications.

Our most important conclusions are as follows.

(i) It is not possible to rule out galaxy assembly bias using SDSS DR7 measurements of $w_{\rm p}$ and $n_{\rm g}$.

(ii) Decorated HOD fits to $w_{\rm p}$ and $n_{\rm g}$ favor significant levels of assembly bias, particularly in the lower luminosity thresholds we study. Both the $M_r < -20, -20.5$ samples prefer relatively strong central galaxy assembly bias.

The $M_r < -19$ sample favors satellite assembly bias. Assembly bias in these samples improves the capability of the model to describe galaxy clustering near the one-halo to two-halo transition at $r_{\rm p} \sim 2\,h^{-1}$Mpc.

(iii) The evidence for galaxy assembly bias weakens for brighter galaxy samples: Decorated HOD fits to the $M_r < -21$ sample are consistent with both $A_{\rm cen} = 0$ and $A_{\rm sat} = 0$. This is consistent with the well-established result that *halo assembly bias* weakens with increasing halo mass over the dynamic range relevant to these galaxy samples (see, e.g., Figure 8 of Hearin et al. 2016, and references therein).

(iv) Our posteriors and best-fit parameters summarized in Table 3.1 supersede the values published in Zehavi et al. (2011), as direct-mock-population together with the Decorated HOD allows us to account for highly significant systematics that have heretofore been neglected from all HOD fits to SDSS data. We note that our findings update the original Zehavi et al. (2011) results *even for our fits to standard HODs without assembly bias*, because the original results were derived from MCMC chains that did not sufficiently sample the HOD model posteriors.

Until such time as we have stringent constraints on the level of assembly bias in the universe, accounting for the possibility of assembly bias is not optional in interpreting galaxy clustering data. Precise statements about galaxy evolution derived from galaxy clustering or attempts to exploit clustering to perform cosmological analyses cannot be made robustly without accounting for assembly bias (see Zentner et al. 2014). Together with the work of Hearin et al. (2016) and the `Halotools` software, we have provided an explicit example of one way forward in such analyses. It is our hope that similar analyses will be performed on forthcoming galaxy survey data and that these analyses will lead to a richer understanding of galaxy evolution and the relationship between galaxies and the halos and environments in which they are found.

6 ACKNOWLEDGEMENTS

We thank Zheng Zheng for his help in diagnosing the differences between the present analysis and the SDSS DR7 analysis presented in Zehavi et al. (2011). We thank Manodeep Sinha for help installing and running the `CorrFunc` package as well as comments on an earlier draft of this manuscript. ARZ and APH are grateful to Prince Rogers Nelson for inspiring our creativity. The authors gratefully acknowledge the Gauss Centre for Supercomputing e.V. (www.gauss-centre.eu) and the Partnership for Advanced Supercomputing in Europe (PRACE, www.prace-ri.eu) for funding the MultiDark simulation project by providing computing time on the GCS Supercomputer SuperMUC at Leibniz Supercomputing Centre (LRZ, www.lrz.de). The Bolshoi simulations have been performed within the Bolshoi project of the University of California High-Performance AstroComputing Center (UC-HiPACC) and were run at the NASA Ames Research Center. The work of ARZ was supported by the US National Science Foundation via grant AST 1517563. FvdB and JUL are supported by the US National Science Foundation through grant AST 1516962. APH is funded through the Yale Center for Astronomy & Astrophysics Prize fellowship.

REFERENCES

Adhikari S., Dalal N., Chamberlain R. T., 2014, JCAP, 11, 19
Behroozi P. S., et al., 2013, ApJ, 762, 109
Behroozi P. S., Wechsler R. H., Wu H.-Y., 2011, ArXiv:1110.4372
Behroozi P. S., Wechsler R. H., Wu H.-Y., Busha M. T., Klypin A. A., Primack J. R., 2013, ApJ, 763, 18
Berlind A. A., Weinberg D. H., 2002, ApJ, 575, 587
Blanton M. R., Berlind A. A., 2007, ApJ, 664, 791
Bryan G. L., Norman M. L., 1998, ApJ, 495, 80
Cacciato M., van den Bosch F. C., More S., Mo H., Yang X., 2013, Mon. Not. R. Astron. Soc., 430, 767
Conroy C., Wechsler R. H., 2009, ApJ, 696, 620
Croton D. J., Gao L., White S. D. M., 2007, Mon. Not. R. Astron. Soc., 374, 1303
Dalal N., White M., Bond J. R., Shirokov A., 2008, ApJ, 687, 12
Foreman-Mackey D., Hogg D. W., Lang D., Goodman J., 2013, PASP, 125, 306
Gao L., Springel V., White S. D. M., 2005, Mon. Not. R. Astron. Soc., 363, L66
Gao L., White S. D. M., 2007, Mon. Not. R. Astron. Soc., 377, L5
Goodman J., Weare J., 2010, Comm. App. Math. and Comp. Sci, 5
Guo H., Zheng Z., Zehavi I., Xu H., Eisenstein D. J., Weinberg D. H., Bahcall N. A., Berlind A. A., Comparat J., McBride C. K., Ross A. J., Schneider D. P., Skibba R. A., Swanson M. E. C., Tinker J. L., Tojeiro R., Wake D. A., 2014, ArXiv:1401.3009
Guo Q., White S., Boylan-Kolchin M., De Lucia G., Kauffmann G., Lemson G., Li C., Springel V., Weinmann S., 2011, Mon. Not. R. Astron. Soc., 413, 101
Hearin A., Campbell D., Tollerud E., Behroozi P., Diemer B., Goldbaum N. J., Jennings E., Leauthaud A., Mao Y.-Y., More S., Parejko J., Sinha M., Sipocz B., Zentner A., 2016, ArXiv:1606.04106
Hearin A. P., Watson D. F., van den Bosch F. C., 2014, ArXiv:1404.6524
Hearin A. P., Zentner A. R., van den Bosch F. C., Campbell D., Tollerud E., 2016, Mon. Not. R. Astron. Soc.
Henriques B. M. B., White S. D. M., Thomas P. A., Angulo R. E., Guo Q., Lemson G., Springel V., 2013, Mon. Not. R. Astron. Soc., 431, 3373
Klypin A., Gottlöber S., Kravtsov A. V., Khokhlov A. M., 1999, ApJ, 516, 530
Lacerna I., Padilla N., 2011, Mon. Not. R. Astron. Soc., 412, 1283
Leauthaud A., et al., 2012, ApJ, 744, 159
Lehmann B. V., Mao Y.-Y., Becker M. R., Skillman S. W., Wechsler R. H., 2015, ArXiv:1510.05651
Lin Y.-T., Mandelbaum R., Huang Y.-H., Huang H.-J., Dalal N., Diemer B., Jian H.-Y., Kravtsov A., 2015, ArXiv:1504.07632

Lu Y., Mo H. J., Katz N., Weinberg M. D., 2012, Mon. Not. R. Astron. Soc., 421, 1779
Lu Y., Mo H. J., Lu Z., Katz N., Weinberg M. D., 2014, Mon. Not. R. Astron. Soc., 443, 1252
Lu Y., Mo H. J., Weinberg M. D., Katz N., 2011, Mon. Not. R. Astron. Soc., 416, 1949
Ma C.-P., Fry J. N., 2000, ApJ, 543, 503
Miyatake H., More S., Takada M., Spergel D. N., Mandelbaum R., Rykoff E. S., Rozo E., 2016, Physical Review Letters, 116, 041301
More S., Diemer B., Kravtsov A. V., 2015, ApJ, 810, 36
More S., Miyatake H., Takada M., Diemer B., Kravtsov A. V., Dalal N. K., More A., Murata R., Mandelbaum R., Rozo E., Rykoff E. S., Oguri M., Spergel D. N., 2016, ArXiv e-prints
More S., van den Bosch F. C., Cacciato M., Mo H. J., Yang X., Li R., 2009, Mon. Not. R. Astron. Soc., 392, 801
More S., van den Bosch F. C., Cacciato M., More A., Mo H., Yang X., 2013, Mon. Not. R. Astron. Soc., 430, 747
Navarro J. F., Frenk C. S., White S. D. M., 1997, ApJ, 490, 493
Paranjape A., Kovač K., Hartley W. G., Pahwa I., 2015, Mon. Not. R. Astron. Soc., 454, 3030
Planck Collaboration Ade P. A. R., Aghanim N., Armitage-Caplan C., Arnaud M., Ashdown M., Atrio-Barandela F., Aumont J., Baccigalupi C., Banday A. J., et al. 2014, Astron. Astrophys., 571, A16
Porciani C., Norberg P., 2006, Mon. Not. R. Astron. Soc., 371, 1824
Riebe K., Partl A. M., Enke H., Forero-Romero J., Gottloeber S., Klypin A., Lemson G., Prada F., Primack J. R., Steinmetz M., Turchaninov V., 2011, ArXiv:1109.0003
Rodríguez-Puebla A., Drory N., Avila-Reese V., 2012, ApJ, 756, 2
Schwarz G., 1978, Ann. Statist., 6, 461
Scoccimarro R., Sheth R. K., Hui L., Jain B., 2001, ApJ, 546, 20
Seljak U., 2000, Mon. Not. R. Astron. Soc., 318, 203
Sinha M., 2016, http://dx.doi.org/10.5281/zenodo.55161
Sunayama T., Hearin A. P., Padmanabhan N., Leauthaud A., 2016, Mon. Not. R. Astron. Soc., 458, 1510
Tinker J. L., Conroy C., Norberg P., Patiri S. G., Weinberg D. H., Warren M. S., 2008, ApJ, 686, 53
Tinker J. L., Leauthaud A., Bundy K., George M. R., Behroozi P., Massey R., Rhodes J., Wechsler R., 2013, ArXiv:1308.2974
Tinker J. L., Weinberg D. H., Zheng Z., Zehavi I., 2005, ApJ, 631, 41
van den Bosch F. C., More S., Cacciato M., Mo H., Yang X., 2013, Mon. Not. R. Astron. Soc., 430, 725
van den Bosch F. C., Yang X., Mo H. J., Weinmann S. M., Macciò A. V., More S., Cacciato M., Skibba R., Kang X., 2007, Mon. Not. R. Astron. Soc., 376, 841
Wake D. A., Whitaker K. E., Labbé I., van Dokkum P. G., Franx M., Quadri R., Brammer G., Kriek M., Lundgren B. F., Marchesini D., Muzzin A., 2011, ApJ, 728, 46
Wang H., Mo H. J., Jing Y. P., 2009, Mon. Not. R. Astron. Soc., 396, 2249
Wang L., Weinmann S. M., De Lucia G., Yang X., 2013, Mon. Not. R. Astron. Soc., 433, 515
Wang Y., Yang X., Mo H. J., van den Bosch F. C., Weinmann S. M., Chu Y., 2008, ApJ, 687, 919
Wechsler R. H., Bullock J. S., Primack J. R., Kravtsov A. V., Dekel A., 2002, ApJ, 568, 52
Wechsler R. H., Zentner A. R., Bullock J. S., Kravtsov A. V., Allgood B., 2006, ApJ, 652, 71
Wetzel A. R., Nagai D., 2015, ApJ, 808, 40
Wetzel A. R., Tinker J. L., Conroy C., van den Bosch F. C., 2014, Mon. Not. R. Astron. Soc., 439, 2687
Yang X., Mo H. J., van den Bosch F. C., 2003, Mon. Not. R. Astron. Soc., 339, 1057
Yang X., Mo H. J., van den Bosch F. C., 2006, Astrophys. J. Lett., 638, L55
Yang X., Mo H. J., van den Bosch F. C., 2009, ApJ, 693, 830
Yang X., Mo H. J., van den Bosch F. C., Zhang Y., Han J., 2012, ApJ, 752, 41
Yang X., Mo H. J., Zhang Y., van den Bosch F. C., 2011, ApJ, 741, 13
Zehavi I., et al., 2005, ApJ, 630, 1
Zehavi I., et al., 2011, ApJ, 736, 59
Zentner A. R., 2007, International Journal of Modern Physics D, 16, 763
Zentner A. R., Hearin A. P., van den Bosch F. C., 2014, Mon. Not. R. Astron. Soc., 443, 3044
Zheng Z., Coil A. L., Zehavi I., 2007, ApJ, 667, 760
Zu Y., Mandelbaum R., 2015, ArXiv:1509.06758